Gyrokinetic Simulation of Turbulent Transport for I-mode Edge Plasmas

Hongwei Yang[1], Tianchun Zhou[2], Yong Xiao[1]

[1]*Institute for Fusion Theory and Simulation, Zhejiang University, Hangzhou 310027, China*

[2]*Harbin Institute of Technology, Harbin 150001, China*

E-mail: yxiao@zju.edu.cn; tczhou@hit.edu.cn

Abstract

I-mode is an attractive candidate among the confinement regimes proposed for burning operation with good energy confinement similar to H-mode but poor particle confinement similar to L-mode, resulting in no obvious impurity accumulation and free of large ELMs. Although I-mode has been recently achieved experimentally on several tokamaks, theory and simulation remain insufficient to explain the I-mode formation and its peculiar transport behavior. In this work, an electrostatic gyrokinetic simulation using GTC is carried out for the I-mode plasma profiles. Linear simulations reveal that two competitive instabilities coexist within the range of short and long wavelengths during I-mode phase, respectively. It is found that the passing electron response cannot be treated adiabatically for those modes with mode numbers close to that of weekly coherent mode (WCM), which is considered to be a major player in the I-mode formation and responsible for its unusual transport behavior. Nonlinear simulations yield a turbulent heat transport level that is comparable to the experimental data. However, the particle transport mechanism remains elusive, and requires further investigation.

Keywords: I-mode, weakly coherent mode, L-I transition

1. INTRODUCTION AND SIMULATION MODEL

I-mode is an intermediate confinement regime in tokamaks between L-mode and H-mode, which was first discovered on ASDEX Upgrade [1] as a transient regime and originally named “Improved L-mode”. During the last decade, researchers on the Alcator C-Mod tokamak have achieved I-mode a stationary operation regime with its lifetime more than 10 times of the energy confinement time τ_E [2]. What makes this regime most special and intriguing is that the energy and particle transport channels in the edge region are decoupled, i.e., it exhibits low energy transport across the last closed flux surface (LCFS), while higher particle transport than that of energy. Furthermore, this regime is free of explosive edge localized modes (ELMs) and as a result of high level of particle transport, there is no apparent impurity accumulation. Thus I-mode is often considered to be an alternative regime for burning plasma operation in parallel with the conventional ELMy or ELM-free H-mode, which needs extra control of impurity accumulation level and strategies for heavy impurities and helium ash removal to avoid significant energy confinement deterioration. To create an I-mode experimentally, people start with L-mode in the magnetic geometry with unfavorable ion $B\times\nabla B$ drift, then L-I transition occur when keeping heating plasmas in various ways with power threshold two times higher than that needed for the direct L-H transition in favorable magnetic geometry, and finally the plasma enters the I-mode regime [3-5]. During this process the edge plasma temperature gradient especially for electrons would increases gradually to the level of the conventional H-modes, while the density gradient changes insignificantly. Meanwhile, edge fluctuations with low frequency disappear and turbulence with broad frequency band pops up in the middle range around 150-400 kHz in lab frame and is believed to play a major role in sustaining the two decoupled transport channels and the whole I-mode regime. These high frequency fluctuations are termed WCM, which can be detected from the signals of fluctuations of density, temperature as well as poloidal magnetic field. Typically, the relative fluctuation level of density in I-mode is about 10%, that of magnetic field less than 1% and that of temperature around 1% [3]. Recently I-mode plasmas with features similar to those on C-Mod have also been created on DIII-D [4, 6], ASDEX Upgrade [3, 6] and EAST [5].

On the theory and simulation side, a few investigators [7-12] have provided some preliminary understandings of I-mode, but challenging issues like the essence of WCM, the mechanism responsible for L-I transition, the decoupling of two transport channels remains to be tackled. Since the long pulse I-mode has been achieved for the first time on C-Mod [13], a tokamak with high toroidal field, people naturally think of high field as an advantage in accessing I-mode as well as sustaining it from transitioning to the H-mode. Recently Whyte et al. have launched a new programme named SPARC [14], which emphasizes particularly the high field approach to burning plasmas, to advance research in this respect. The primary goal of this paper is to investigate the fluctuations and their transport properties in the I-mode plasmas through massive gyrokinetic simulations using GTC (Gyrokinetic Toroidal Code) [15]. We have conducted a series of global gyrokinetic simulations, using the profiles from the discharge #1120907023 on Alcator C-Mod [6, 7, 16]. Since in the I-mode plasmas the density fluctuation level is much higher than that of magnetic fluctuation [3, 9] and the local β_e is estimated to be less than 0.1% around the temperature pedestal of the I-mode, the electrostatic approximation will be adopted as a first attempt of our I-mode study via gyrokinetic simulation. Given the characteristic frequencies and wavelengths of the I-mode plasma fluctuations, the ion response is described by gyrokinetics and that of the electron by drift kinetics [17, 18], and both passing and trapped particles are retained in the simulation.

The simulation domain is restricted in the edge region of tokamak around 0.8~0.99 minor radius of the plasma column with $R_0 = 0.67m$, $a = 0.22m$, where the WCM and temperature pedestal are located. The two normalized gradient length scales of local electron and ion temperatures are taken as $R_0/L_{Te} = R_0/L_{Ti} = 142$, and those of local density as

$R_0/L_{ne} = R_0/L_{ni} = 42$. Other parameters adopted are $T_{e,95} = 700eV$, $n_{e,95} = 1\times10^{20} m^{-3}$, local safety factor $q_{95} = 3.5$ and on-axis magnetic field $B_0 = 5.8T$, which gives rise to the local ratio $a/\rho_s = 472$ with gyroradius $\rho_s \equiv C_s / \Omega_c$ at the reference point, where ion sound speed $C_s \equiv \sqrt{T_e / m_p}$, m_p is proton mass and $\Omega_c = eB_0 / m_p$. We select deuterium (D) as the main ion species in the simulation. By ignoring plasma shaping, the magnetic flux surfaces are simply assumed to be concentrically circular.

2. VALIDATION OF I-MODE EDGE PROPERTIES

To validate nonlinear GTC simulation, we need to compare turbulence characteristics and transport level from the simulation with the experimental features exhibited in I-mode plasmas. Here we list a number of important characteristics of the I-mode plasmas from C-Mod discharge #1120907023 [6]: there exists characteristic turbulent fluctuations called WCM, which propagate in electron diamagnetic drift (EDD) direction with frequency around 150-400kHz in the lab frame; it is also observed that a geodesic acoustic mode (GAM) coexists with the WCM; the turbulent effective heat conductivity is measured to be about $0.2m^2/s$, and the particle transport is four times larger [7, 19].

As shown in Fig. 2, our nonlinear simulation successfully demonstrates that the nonlinear edge heat conductivities for ion and electron, χ_i and χ_e, are in the same level as the experimental values. However, the particle diffusivities for both species, D_i and D_e, are significantly lower than those from experiment diagnostics. This suggests that the particle and energy transport decoupling observed in the I-mode experiment cannot be reproduced by our gyrokinetic simulation in the electrostatic limit. This further implies that the dominant turbulence such as the WCM could not be completely treated as electrostatic, although the edge density fluctuation level of WCM is one order of magnitude higher than that of poloidal magnetic field and the edge local β_e value is small enough so that the traditional drift wave turbulence can be safely treated as electrostatic. Surprisingly, we found that the turbulence driven by the I-mode profiles can self-generate GAM oscillations and low frequency zonal flow (LFZF), that have been observed in all I-mode experiments [20, 21]. Shown in Fig. 3 (a) & (b) are the evolution of the perturbed electrostatic potential averaged over the reference magnetic surface, where the change of color with time over the narrow edge region in the form of strips indicates that there exists the component of oscillations with mode numbers $n=0$ and $m=0$, which is for GAM and LFZF. Simple estimation based on the periodic change shown in Fig. 3 (a) & (b) reveals that the frequency normalized to GAM frequency predicted from ideal magneto-hydrodynamics (MHD) in high safety factor q region is $\omega_{GAM}^{simulation} \simeq 1.45\omega_{GAM}^{MHD}$ with $\omega_{GAM}^{MHD} \approx \sqrt{2}(1+q^{-2}/2)C_s/R_0$ and $C_s \equiv \sqrt{T_e/m_p}$ [22], which is very close to the characteristic order of GAM. Shown in Fig. 4 is the frequency spectrum during nonlinear saturation process in the temporal window bounded by the two vertical dashed lines in Fig. 5, which ranges over a WCM-like signal near the frequency $4.8C_s/R_0$, a GAM signal near the frequency $1.6C_s/R_0$ and extremely low frequency for LFZF.

3. TURBULENCE SATURATION MECHANISMS AND ROLES OF GAM/LFZF

In this set of nonlinear validation simulations, we find out that the turbulence saturates twice in succession, one phase of gently linear growth and saturation followed by another phase of more explosive linear growth and saturation, which is somewhat atypical, as illustrated by the blue solid line in Fig. 5 for time evolution of the electron heat conductivity . This suggests that there may exist two distinct instabilities in two consecutive stages which are labeled respectively as the first and second instabilities. The first instability dominates the earlier nonlinear process and the second one dominates the later phase. In a typical nonlinear saturation process, the dominant unstable mode, which is the most unstable one determined by linear dispersion relation, undergoes exponential growth and gets saturated by wave-wave interaction or wave-particle interaction [15, 23], then the turbulent plasma enters the nonlinear saturation stage and stays in steady state. However, in the nonlinear processes shown in Figs. 4 and 5, right after the first instability becomes saturated and its level gets lowered down somewhat by some dissipation for a while, the second instability is then excited and takes over. Then the energy transport levels for both species are boosted by another explosive growth of the second instability, to much higher level, e.g., about five times that of the first stage, when new nonlinear saturation is reached.

To verify our theory that the two instabilities are of different types, we need to examine the time evolution of mode wavelength for each of them in nonlinear process, that is, we need to analyze their poloidal mode spectra, as is exhibited in Fig. 6. Around $t=2.5R_0/C_s$ in Fig.6 (a), the first unstable mode grows exponentially which correspond to the first uphill of the blue/solid curve in Fig.5 with central perpendicular wavenumber $k_\theta\rho_s \approx 0.8776$ shown by the vertical dashed lines in Fig. 6 (a) & (b). This wavelength is comparable to that of trapped electron mode (TEM), which is a typical short wavelength instability, whereas this poloidal wavelength is shorter than that inferred from the WCM. Around $t=3.75R_0/C_s$, as is shown in Fig. 6 (b) which corresponds to the first downhill of the blue/solid curve in Fig.5， the spectrum peaks at $k_\theta\rho_s \approx 0.13$ as is marked by the left vertical dashed line. Meanwhile, the peaks around $k_\theta\rho_s \approx 0.8776$ are dwindling drastically relative to the surroundings. We note that $k_\theta\rho_s \approx 0.13$ is very close to the measured poloidal wavenumber of WCM reported in [24]. This means the energy carried by the modes with short wavelengths has been inversely cascaded to the long wavelength WCM-like modes. Around $t=6R_0/C_s$ and afterwards, the second instability undergoes an exponential growth and reaches a much higher saturation level as is shown in Fig. 5 and Fig. 6 (c), and the value of $k_\theta\rho_s$ is eventually locked around

0.13, which is consistent with the poloidal wavenumber of WCM in the experiment. During the growth of second linear instability and nonlinear saturation the first instability with $k_\theta\rho_s \approx 0.8776$ disappears completely in the poloidal spectra.

On the other hand, when we use some numerical technique to filter out those modes with short wavelengths around $k_\theta\rho_s \approx 0.8776$ corresponding to toroidal mode number $n \geq 50$ in our nonlinear simulation, the results plotted in Fig. 7 illustrate that, although the first stage of linear growth and saturation disappears, the final saturation levels of both heat conductivities and particle diffusivities do not change significantly, comparing with those simulations with short wavelength modes retained. Whether or not the first instability is filtered out, the electrostatic fluctuating potential for WCM turbulence maintains almost the same level, and the turbulence potential cascade nonlinearly into the same type of long wavelength mode with $k_\theta\rho_s \approx 0.13$. This indicates that although the first stage exponential growth of the modes with shorter wavelength ($n \geq 50$) raises the transport level by a small amount, apparently, they do not play determining role when the system evolves into the ultimate nonlinear saturation phase. Therefore, between the two instabilities with distinct spatial scales, it is the mode with $k_\theta\rho_s \approx 0.13$ that behaves like WCM in the I-mode determines the transport level, and hence could be identified as the WCM.

It is well-known that GAM/LFZF has the capability of regulating turbulence and improving confinement quality indirectly. One naturally expects that the regulation of GAM/LFZF remains valid for the I-mode. In fact, the experiments [21, 23] have revealed that: (1) GAM sucks energy from the WCM turbulence and broadens the frequency band of the latter through nonlinear interaction; (2) GAM and WCM vanishes simultaneously when the plasmas change from I-mode to flow-up ELM-free H-mode when heating power is above some threshold [2, 3, 19]. However, it remains elusive to what extent the regulating role is played by GAM/LFZF in I-mode plasmas. We therefore conduct two contrasting nonlinear simulations to examine the influences of GAM/LFZF on WCM and its transport properties. In one of such simulations, we calculate the electron heat conductivity induced by the WCM turbulence with the self-generated GAM/LFZF retained and the time history of this transport coefficient is plotted in Fig. 5 as blue/solid curve, in the other the response of GAM/LFZF is filtered out and the resultant electron heat conductivity by turbulence alone is shown in Fig. 5 as red/dashed curve. By turning on and off the contributions of GAM/LFZF response, we find out that both the first and second instabilities are strongly regulated by them. However， the second instability is evidently more affected, as not only its saturation level drops down more but also it oscillates more violently, after reaching its peak value when entering the nonlinear phase.

4. LINEAR PHYSICS OF I-MODE

Following the traditional procedure of exploring generic nonlinear physics, in order to gain deeper understanding of WCM turbulence, it is not sufficient to work on the nonlinear simulation alone. In fact, we conduct a series of linear simulations to see how the linear dispersion relation behaves and to identify the dominant unstable mode at each linear stage of the two distinct evolution processes in our previous nonlinear simulation.

4.1 Linear Dispersion Relation for the Instabilities

In our linear simulations, we first work on single fixed toroidal mode number n to capture the most unstable poloidal mode, and then vary the n number to get the frequency and linear growth rate for each mode that needs to be identified. Firstly, we retain all ingredients of gyrokinetic ion response and all those of drift-kinetic electron in our linear simulations. In this case, as is shown in Fig. 8 (b), there are two comparable peaks of linear growth rate, whose location are very close to $k_\theta \rho_s \approx 0.16$ and $k_\theta \rho_s \approx 0.85$, respectively, i.e., the two normalized poloidal wave numbers marked in Fig. 6 for the two dominant instabilities in preceding nonlinear simulations. Thus, the mode with maximum growth rate around $k_\theta \rho_s \approx 0.85$ corresponds to the first exponentially growing phase shown in Fig. 5, and the one with peaked growth rate around $k_\theta \rho_s \approx 0.16$ to the second linear growing phase in Fig. 5, which accounts for the WCM observed in experiment [24]. Moreover, we note that the linear growth rate for the mode with $k_\theta \rho_s \approx 0.85$ is slightly larger than that with $k_\theta \rho_s \approx 0.16$, and the first unstable mode grows faster and saturates earlier. This is also consistent with our previous observation for the dynamic evolution of these two modes in the nonlinear saturation process, that is, the more unstable mode exponentially grows faster and saturates earlier in nonlinear evolutions.

Upon inspecting the mode frequencies and the directions of phase velocity shown in Fig. 8 (a)， we find out that there are three categories of modes: (1) the most unstable modes with $k_\theta \rho_s \approx 0.85$, which is marked as the "1st unstable" in Fig. 8 (b) and propagates in EDD with frequencies in the range of typical ion scale drift instabilities such as TEM; (2) the unstable mode with $k_\theta \rho_s \approx 0.16$, which is marked as "2nd unstable" in Fig. 8 (b), and also propagates in EDD with frequency close to the electron transit frequency ω_{te}; (3) the unstable modes with poloidal wave numbers somewhere between previous two types ($0.4 < k_\theta \rho_s < 0.8$), which propagates in the ion diamagnetic drift direction (IDD) and have frequencies close to the frequency ω_{*i} or frequency of typical ion drift waves, such as ion temperature gradient (ITG) mode. Furthermore, upon switching off the non-adiabatic response of passing electrons and keeping the trapped electron response only, we find out that only the second type unstable mode (the type with highest frequency) are sensitively affected in such a way that both its frequency and linear growth rate drop down substantially. On the other hand, it is well-known that the passing electron response is close to adiabatic for typical ion drift waves, and the dispersion relation of this type of modes is not expected to be affected sensitively by switching on or off the non-adiabatic passing electron response. The existence of significant non-adiabatic response for the passing electron indicates that the second instability, consistent with the WCM observed experimentally in mode frequency, wavelength, as well as propagation direction, belongs to the certain type of instabilities different from conventional drift waves.

Based on the preceding facts, we conclude that the high frequency branch with longer wavelength ($k_\theta\rho_s \approx 0.16$) is unlikely to be either TEM or ITG, while the low frequency branch with shorter wavelength ($k_\theta\rho_s \approx 0.85$) should be TEM. In addition, when the ion temperature gradient is lowered down to be comparable to that of ion density ($\eta_i \simeq 1$), shown as the red/dashed curves in Fig. 9, the high frequency branch persists with slight upswing of frequency. Thus, it is fair to say that the contribution of ion temperature gradient to this branch is not very relevant. So ITG mode must be ruled out as the candidate for WCM at least in the sense of linear instability drive.

4.2 I-mode Formation Mechanism

Now we focus on the high frequency mode of with $k_\theta\rho_i = 0.16$ or $n = 20$, which is the typical toroidal mode number of WCM observed in the C-Mod experiment [24]. As has been checked in Subsection 4.1, the existence of this branch is insensitive to the ion temperature gradient, thus it can be safely frozen by setting $\eta_i = 1.0$ in the following analysis. We decrease η_e from 4.0 to 1.0 by reducing the electron temperature gradient while keeping electron density gradient fixed. Here the smallest value 1.0 for η_e corresponds to the electron profiles that are almost the same as those of ions, a situation resembling the back transition from I-mode to L-mode. As shown in Fig. 10 (a), whether or not the passing electron response is retained in the simulation, there always exists a narrow threshold band of η_e centered around $\eta_{ec} \simeq 2.0$, across which the L-I transition occurs, indicated by the big mode frequency jump. Below this band, the influence of non-adiabatic response of passing electron on the viable instability becomes irrelevant and the corresponding instability should be TEM that propagates with characteristic frequency around ω_{*e} in EDD. Meanwhile, the plasma profiles degrade to those for a typical L-mode plasma, which agrees with the common picture that TEM grows most easily at the plasma edge for the L-mode plasmas. However, as η_e is increased above the threshold band, the mode frequency jumps up abruptly to the values that are close to the electron transit frequency ω_{te}, which is located in the range of the higher frequency branch aforementioned in Section 3 and Subsection 4.1. Moreover, for a wide range of η_e above the threshold band, the non-adiabatic response of passing electrons produces a huge change in the mode frequency as well as a mild change in the growth rate. The heavy dependence on passing electrons excludes this mode from some typical drift wave instabilities such as TEM. In this range the plasma profiles become similar to those of I-mode plasmas. As we know, the typical I-mode plasmas come along with the existence of temperature barrier and the absence of particle barrier in the edge region, which complies with a large edge temperature gradient or η_e. Thus, the mode-jumping across critical values of η_e may be relevant to the transition mechanism from L-mode to I-mode or vice versa, and in terms of frequency range, the high frequency mode or its derivative mode is likely to account for the WCM widely observed in the I-mode plasmas. All these similarities cannot easily be counted as just coincidences. Instead, there are new evidences that the high frequency mode is indeed WCM, besides those offered by the nonlinear simulations.

5. COLLISIONAL EFFECTS

So far collisionality has been completely ignored in our simulation. In the I-mode plasmas, the density profile becomes flat, and the edge temperature is significantly lower than the core temperature, which is similar to conventional H-mode plasmas. The edge collisionality is expected to be higher than that in the core region and the edge plasmas may not be collisionless. Hence, it is better to check how the collisionality affects the instability and transport in the I-mode plasmas. To this end, we add collisional effects by implementing a pitch-angle scattering process for electrons in the simulation, the local effective electron collision frequency ν_e^* is found to be $\nu_e^* \approx 0.33$ according to Ref. [25-27]. The nonlinear simulation is repeated for this collisional case, and the heat conductivity, particle diffusivity and GAM/LFZF saturation level are shown in Fig. 11 (a), (b) & (c). These are contrast plots for the electron heat conductivities, electron particle diffusivities, and GAM/LFZF saturation levels from the fluctuations of electrostatic potential respectively, between the case with collisions (red dashed curve) and the case without collisions or collisionless (blue solid curve). The downshifts of the two transport coefficients at each time step and the delayed peaks reveal that both the first and second instabilities are partially stabilized by the electron collisional effects. In particular, the nonlinear saturation level of the second instability is lowered down by the collisional effects more enormously and significantly. This difference can also be detected from the GAM/LFZF saturation levels, see Fig. 11 (c). For the first exponential growth and saturation, the collisional effect on the GAM/LFZF is marginal. But for the second one, GAM/LFZF are visibly damped by the electron collision, in which the turbulence was supposed to induce more severe transport than the collisionless case [28, 29]. In fact, we observe the contrary trend in the transport level, i.e., the turbulent transport with physical collisions is less than the collisionless turbulent transport shown in Fig. 11 (a) & (b), which suggests much less linear drive in the case with collisions and the damping effect of collisions play a major role. Therefore, the electron collisional effect in this I-mode scenario is different from that in either dissipative trapped electron mode (DTEM) or resistive ballooning mode (RBM), since both DTEM and RBM are normally destabilized by collisional effects in this weak collisional regime. Based on the preceding observations and considerations, both DTEM and RBM can be excluded from the candidates of WCM.

6. SUMMARY AND DISCUSSION

In this paper we present a novel understanding of the mechanism of I-mode formation and the essence of the associated WCM, based on our electrostatic GTC simulations with the profiles that are taken directly from the experimental I-mode data on C-Mod. In particular, our nonlinear simulations have two major findings: (1) a long wavelength instability with high frequency in the typical range of local electron transit frequency ω_{te} dominates the nonlinear evolution of the I-mode edge plasmas, and this instability resembles WCM in I-mode plasmas in many aspects, such as mode wavelength, frequency spectra of edge fluctuations, energy transport levels and characteristics of profiles evolution from L-mode to I-mode transitions; (2) GAM oscillations with characteristic frequency close to $\omega_{GAM}^{MHD} \approx \sqrt{2}(1+q^{-2}/2)C_s/R_0$ are identified to be self-generated by the turbulence nonlinear interaction. Up to now, almost all I-mode experiments have observed [5, 21, 30] that GAM co-exists with WCM fluctuations when plasmas transition from L-mode to I-mode occurred. To our best knowledge, this is the first time that this universal experimental phenomenon has been verified from our first principle gyrokinetic simulations. Meanwhile, the level of effective heat conductivity out of our simulations is consistent with the experimental values. All these successes strongly suggest that we have captured many essential physics of the I-mode plasmas, except that the particle transport level from our simulation is too low to justify the transport decoupling. This imply that the transport decoupling of I-mode cannot be reproduced in the electrostatic simulation. To see this decoupling, we need to resort to electromagnetic simulation.

As for the linear simulation on I-mode, we have discovered a newly high frequency unstable mode exhibiting many features that are similar to those for WCM in our linear simulation results. In particular, this mode has a frequency in the range of local electron transit frequency ω_{te} in the plasma frame and propagates in EDD. The mode wavelength is also similar to that of WCM. These two features owned simultaneously by the instability: high frequency (fast time scale), long wavelength (large space scale) and the non-adiabatically passing electron response exclude TEM, especially collisionless trapped electron mode (CTEM) as a candidate for WCM in I-mode plasmas. Furthermore, we find out that finite electron collisional effects can stabilize this mode, so both DTEM and RBM are ruled out. Moreover, since the growth rate of this mode is not sensitive to the local value of η_i , ITG mode is also ruled out as the dominant linear instability for WCM. By varying the scale length of electron temperature and density gradient, we have pinpointed the high frequency mode down to an instability, driven by electron temperature gradient with long wavelength and high frequency. All these features strongly suggest that there exist a new type of instability sustaining the I-mode, which is, however, not listed in the zoo of instabilities ever documented before (see, e.g., [31]). Further analytical and numerical studies are desired to give a clear identification of this mode.

ACKNOWELEDGMENTS

This work is supported by NSFC under Grant NO. 11975201, National Magnetic Confinement Fusion Energy Research Program of China under Grant No. 2015GB110000.

Figures

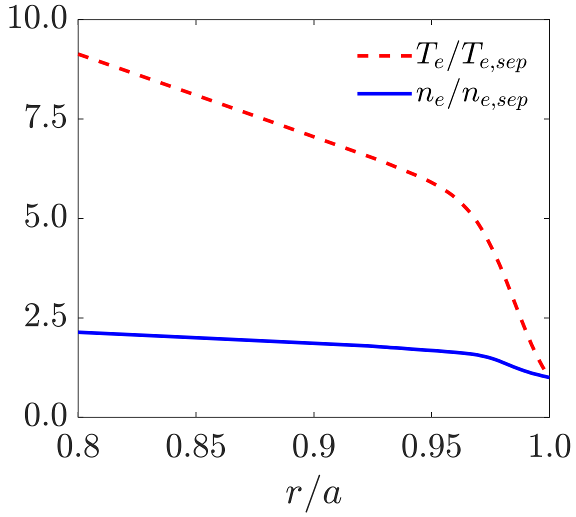

Fig. 1 Edge profiles of I-mode [6].

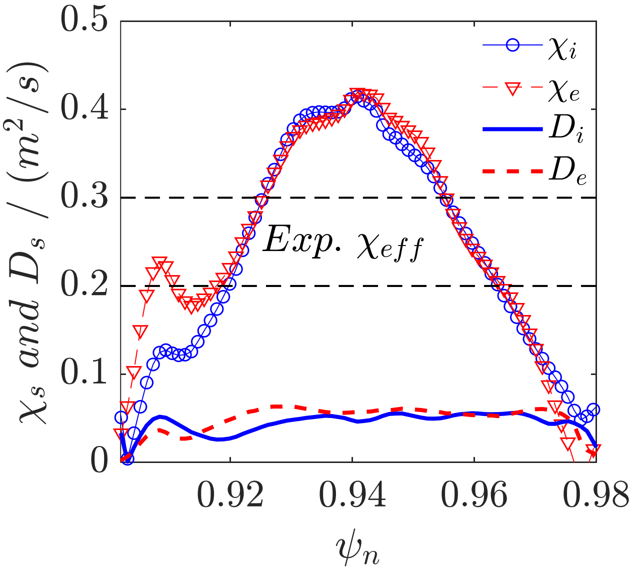

Fig. 2 Radial profiles of ion/electron heat conductivities χ_i / χ_e *and particle diffusivities* D_i / D_e.

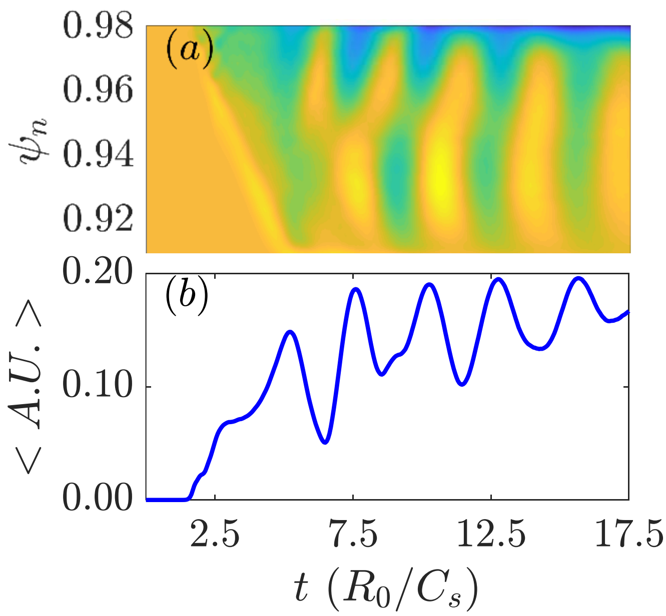

Fig. 3 (a) Radial structures of GAM/LFZF and their time evolutions; (b) time evolution of GAM/LFZF intensity at the diagnostic point $r = r_{ref}, \theta = 0, \zeta = 0$.

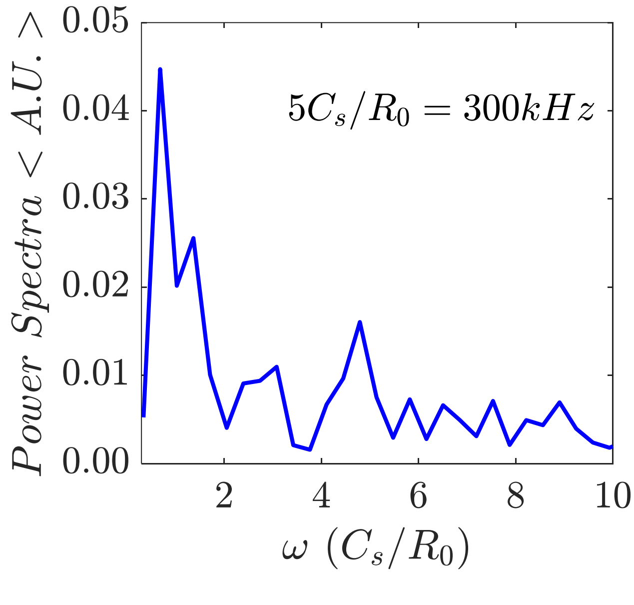

Fig. 4 Power spectrum of electrostatic potential at $r = r_{ref}$, $\theta = 0$ *and* $\zeta = 0$. *The peaks around* $\omega = 0.5, 1.4, 4.8$ *(in unit* C_s / R_0 *) are identified with LFZF, GAM and WCM, respectively.*

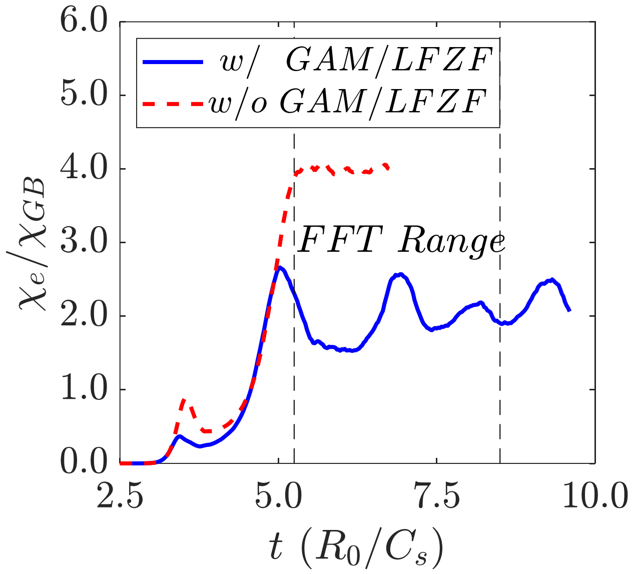

Fig. 5 Time evolution of electron heat conductivities induced by WCM and the regulation by GAM/LFZF on it. Bounded by the two vertical dashed lines is the time in which the power spectra over frequency has been analyzed, as shown in Fig. 4.

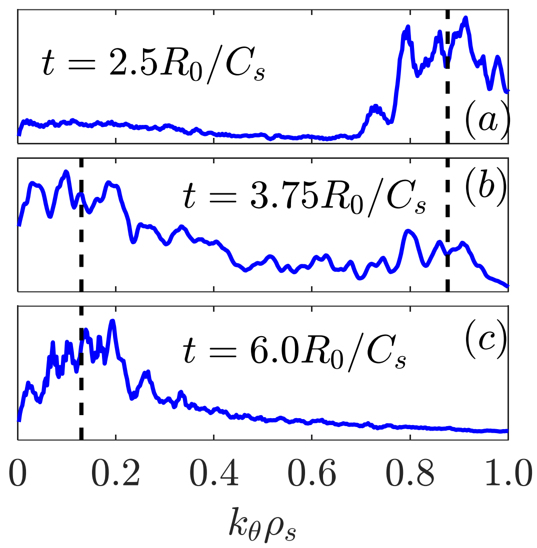

Fig. 6 Poloidal spectra measured at three moments corresponding to those on the blue/solid curve in Fig. 5.

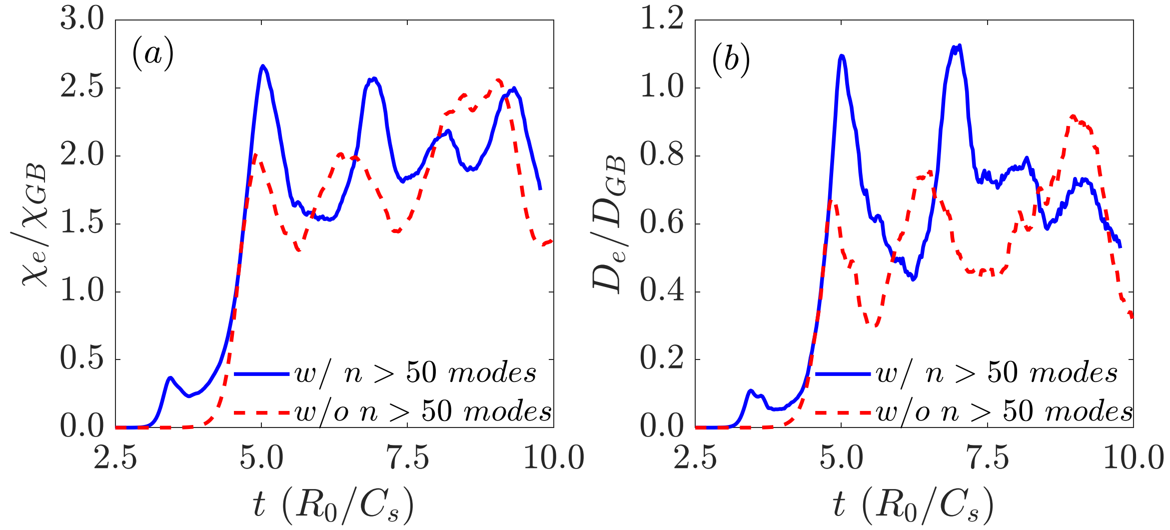

Fig. 7 Simulation with filtering out short wavelength modes have the same saturation level as that retaining full poloidal spectral. (a), Time history of electron heat conductivity. (b), Time history of electron particle diffusivity.

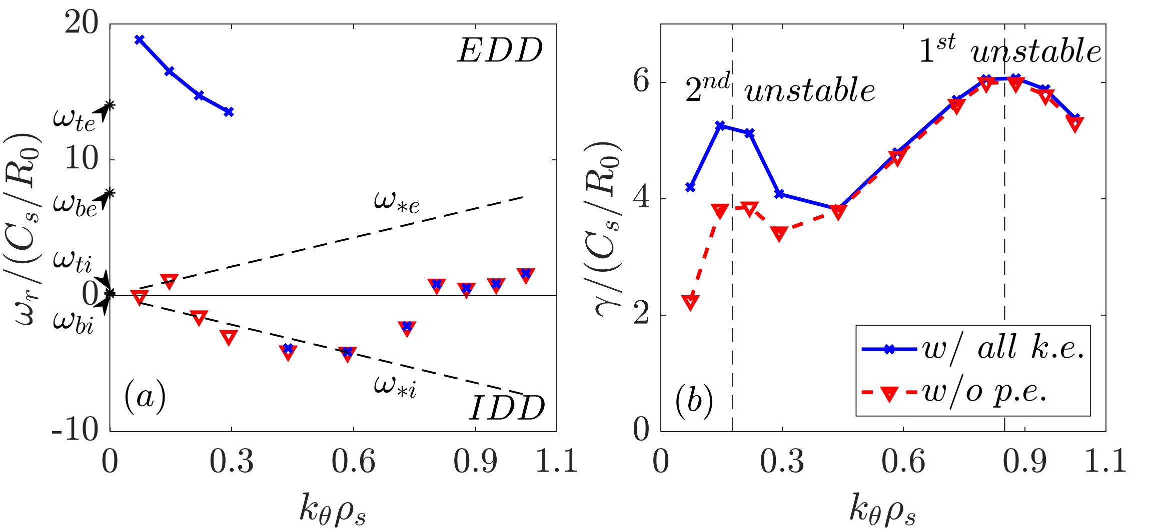

Fig. 8 Linear dispersion relations of I-mode edge plasmas. (a), Real frequency ω_r vs. $k_\theta\rho_s$. (b), Linear growth rate γ vs. $k_\theta\rho_s$. Positive ω_r corresponds to the poloidal mode phase velocity in EDD. Marked on ω_r-axis with asterisks are the heights of ω_{te}, ω_{be}, ω_{ti} and ω_{bi}. The blue crosses are for the case retaining non-adiabatic response of passing electrons while the red triangles for the case with that being turned off.

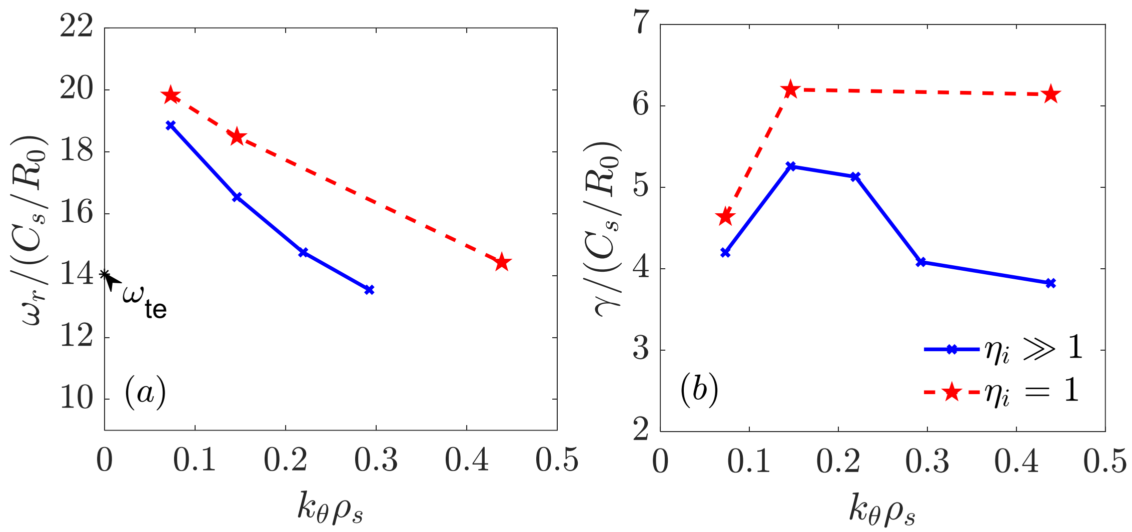

Fig. 9 η_i *-sensitivity of the higher frequency mode. (a), Real frequency* ω_r *vs.* $k_\theta\rho_s$*. (b), Linear growth rate* γ *vs.* $k_\theta\rho_s$*. The blue cross is for the case with the value of* η_i *calculated from the I-mode profiles, i.e.* $\eta_i \gg 1$*, while the red star for the case with* $\eta_i = 1$.

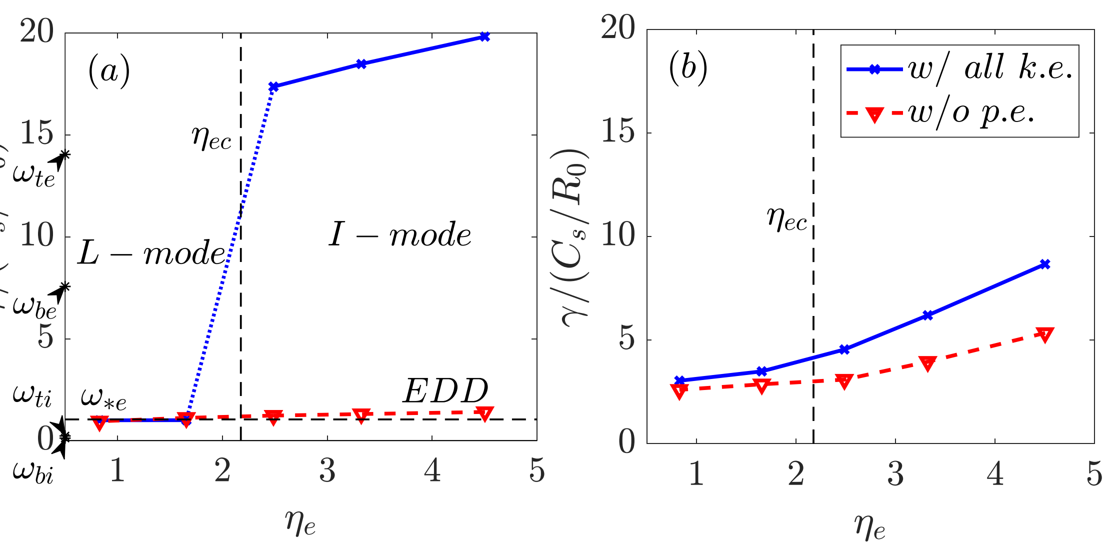

Fig. 10 L-I transition and instability-jumping as η_e *crosses critical values. (a) Real frequency* ω_r *vs.* $k_\theta\rho_s$*; (b) Linear growth rate* γ *vs.* $k_\theta\rho_s$.

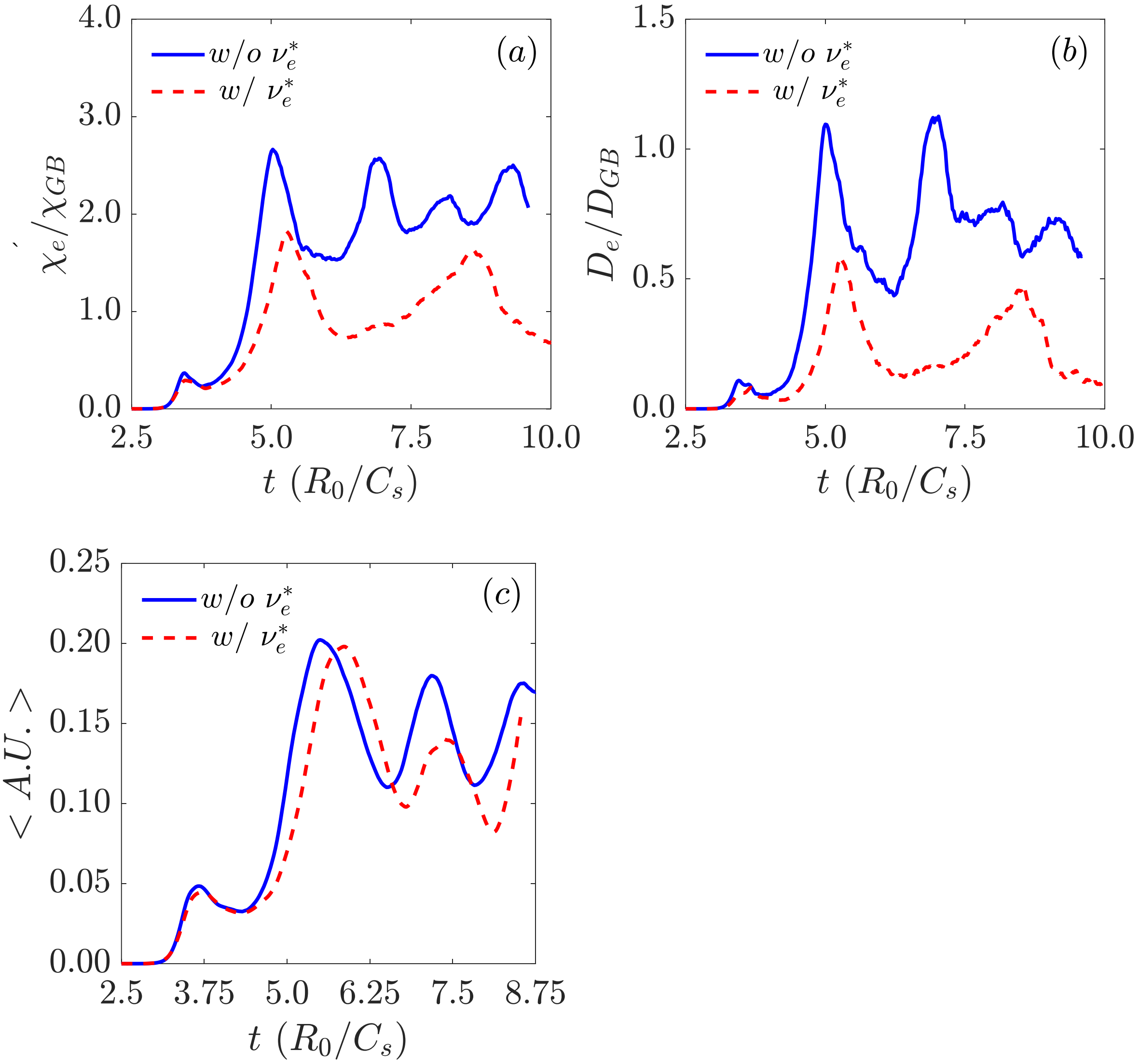

Fig. 11 Electron collisional effects on the transport properties in I-mode. (a), The electron heat conductivity is lowered by collisional effects. (b), The electron particle diffusivity is lowered by collisional effects. (c), The GAM/LFZF saturation level is lowered by collisional effects

REFERENCES

[1] Ryter F, Suttrop W, Brusehaber B, Kaufmann M, Mertens V, Murmann H, Peeters A G, Stober J, Schweinzer J, Zohm H and Team A U 1998 H-mode power threshold and transition in ASDEX Upgrade *Plasma Physics and Controlled Fusion* **40** 725-9

[2] Whyte D G, Hubbard A E, Hughes J W, Lipschultz B, Rice J E, Marmar E S, Greenwald M, Cziegler I, Dominguez A, Golfinopoulos T, Howard N, Lin L, McDermott R M, Porkolab M, Reinke M L,

Terry J, Tsujii N, Wolfe S, Wukitch S, Lin Y and Team A C-M 2010 I-mode: an H-mode energy confinement regime with L-mode particle transport in Alcator C-Mod *Nuclear Fusion* **50**

[3] Ryter F, Fischer R, Fuchs J C, Happel T, McDermott R M, Viezzer E, Wolfrum E, Orte L B, Bernert M, Burckhart A, da Graca S, Kurzan B, McCarthy P, Putterich T, Suttrop W, Willensdorfer M and Team A U 2017 I-mode studies at ASDEX Upgrade: L-I and I-H transitions, pedestal and confinement properties *Nuclear Fusion* **57**

[4] Marinoni A, Rost J C, Porkolab M, Hubbard A E, Osborne T H, White A E, Whyte D G, Rhodes T L, Davis E M, Ernst D R, Burrell K H and Team D-D 2015 Characterization of density fluctuations during the search for an I-mode regime on the DIII-D tokamak *Nuclear Fusion* **55**

[5] Feng X, Liu A D, Zhou C, Liu Z X, Wang M Y, Zhuang G, Zou X L, Wang T B, Zhang Y Z, Xie J L, Liu H Q, Zhang T, Liu Y, Duan Y M, Hu L Q, Hu G H, Kong D F, Wang S X, Zhao H L, Li Y Y, Shao L M, Xia T Y, Ding W X, Lan T, Li H, Mao W Z, Liu W D, Gao X, Li J G, Zhang S B, Zhang X H, Liu Z Y, Qui C M, Zhang S, Zhang J, Ji J X, Fan H R and Zhong X M 2019 I-mode investigation on the Experimental Advanced Superconducting Tokamak *Nuclear Fusion* **59**

[6] Hubbard A E, Osborne T, Ryter F, Austin M, Orte L B, Churchill R M, Cziegler I, Fenstermacher M, Fischer R, Gerhardt S, Groebner R, Gohil P, Happel T, Hughes J W, Loarte A, Maingi R, Manz P, Marinoni A, Marmar E S, McDermott R M, McKee G, Rhodes T L, Rice J E, Schmitz L, Theiler C, Viezzer E, Walk J R, White A, Whyte D, Wolfe S, Wolfrum E, Yan Z, Team A C-M, Team A U and Team D-D 2016 Multi-device studies of pedestal physics and confinement in the I-mode regime *Nuclear Fusion* **56**

[7] Liu Z X, Xu X Q, Gao X, Hubbard A E, Hughes J W, Walk J R, Theiler C, Xia T Y, Baek S G, Golfinopoulos T, Whyte D, Zhang T and Li J G 2016 The physics mechanisms of the weakly coherent mode in the Alcator C-Mod Tokamak *Physics of Plasmas* **23**

[8] White A E, Howard N T, Creely A J, Chilenski M A, Greenwald M, Hubbard A E, Hughes J W, Marmar E, Rice J E, Sierchio J M, Sung C, Walk J R, Whyte D G, Mikkelsen D R, Edlund E M, Kung C, Holland C, Candy J, Petty C C, Reinke M L and Theiler C 2015 Nonlinear gyrokinetic simulations of the I-mode high confinement regime and comparisons with experiment *Physics of Plasmas* **22**

[9] Mikkelsen D R, Howard N T, White A E and Creely A J 2018 Verification of GENE and GYRO with L-mode and I-mode plasmas in Alcator C-Mod *Physics of Plasmas* **25**

[10] Manz P, Happel T, Stroth U, Eich T, Silvagni D and Team A U 2020 Physical mechanism behind and access to the I-mode confinement regime in tokamaks *Nuclear Fusion* **60**

[11] liu X 2018 Gyrokinetic simulation of pedestal turbulence using GENE. The University of Texas at Austin) p 126 p.

[12] Coppi B and Zhou T 2012 Interpretation of the I-Regime and transport associated with relevant heavy particle modes *Physics of Plasmas* **19**

[13] Hubbard A E, Whyte D G, Churchill R M, Cziegler I, Dominguez A, Golfinopoulos T, Hughes J W, Rice J E, Bespamyatnov I, Greenwald M J, Howard N, Lipschultz B, Marmar E S, Reinke M L, Rowan W L, Terry J L and Grp A C-M 2011 Edge energy transport barrier and turbulence in the I-mode regime on Alcator C-Mod *Physics of Plasmas* **18**

[14] Whyte D 2019 Small, modular and economically attractive fusion enabled by high temperature superconductors *Philos T R Soc A* **377**

[15] Lin Z, Hahm T S, Lee W W, Tang W M and White R B 1998 Turbulent transport reduction by zonal flows: Massively parallel simulations *Science* **281** 1835-7

[16] Walk J, Hughes J, Hubbard A, Whyte D and White A 2015 Impact of the Pedestal on Global Performance and Confinement Scalings in I-mode. In: *Aps Meeting,*

[17] Lin Z H and Chen L 2001 A fluid-kinetic hybrid electron model for electromagnetic simulations *Physics of Plasmas* **8** 1447-50

[18] Lin Z, Nishimura Y, Xiao Y, Holod I, Zhang W L and Chen L 2007 Global gyrokinetic particle simulations with kinetic electrons *Plasma Physics and Controlled Fusion* **49** B163-B72

[19] Cziegler I, Diamond P H, Fedorczak N, Manz P, Tynan G R, Xu M, Churchill R M, Hubbard A E, Lipschultz B, Sierchio J M, Terry J L and Theiler C 2013 Fluctuating zonal flows in the I-mode regime in Alcator C-Mod *Physics of Plasmas* **20**

[20] Dimits A M, Bateman G, Beer M A, Cohen B I, Dorland W, Hammett G W, Kim C, Kinsey J E, Kotschenreuther M, Kritz A H, Lao L L, Mandrekas J, Nevins W M, Parker S E, Redd A J, Shumaker D E, Sydora R and Weiland J 2000 Comparisons and physics basis of tokamak transport models and turbulence simulations *Physics of Plasmas* **7** 969-83

[21] Cziegler I, Hubbard A E, Hughes J W, Terry J L and Tynan G R 2017 Turbulence Nonlinearities Shed Light on Geometric Asymmetry in Tokamak Confinement Transitions *Physical Review Letters* **118**

[22] Winsor and Niels 1968 Geodesic Acoustic Waves in Hydromagnetic Systems **11** 2448-0

[23] Cziegler I 2011 Turbulence and transport phenomena in edge and scrape-off-layer plasmas. Massachusetts Institute of Technology) p 178 p.

[24] Dominguez A 2012 Study of density fluctuations and particle transport at the edge of I-mode plasmas. Massachusetts Institute of Technology) p 208 p.

[25] Hinton F L and Hazeltine R D 1976 Theory of Plasma Transport in Toroidal Confinement Systems *Reviews of Modern Physics* **48** 239-308

[26] Huba J D, United States. Office of Naval Research. and Naval Research Laboratory (U.S.) 2009 NRL plasma formulary. (Washington, DC: Naval Research Laboratory ,) p 1 online resource (71 pages)

[27] Sauter O, Angioni C and Lin-Liu Y R 1999 Neoclassical conductivity and bootstrap current formulas for general axisymmetric equilibria and arbitrary collisionality regime *Physics of Plasmas* **6** 2834-9

[28] Hinton F L and Rosenbluth M N 1999 Dynamics of axisymmetric (E x B) and poloidal flows in tokamaks *Plasma Physics and Controlled Fusion* **41** A653-A62

[29] Xiao Y, Catto P J and Molvig K 2007 Collisional damping for ion temperature gradient mode driven zonal flow *Physics of Plasmas* **14**

[30] Manz P, Lauber P, Nikolaeva V E, Happel T, Ryter F, Birkenmeier G, Bogomolov A, Conway G D, Manso M E, Maraschek M, Prisiazhniuk D and Viezzer E 2015 Geodesic oscillations and the weakly coherent mode in the I-mode of ASDEX Upgrade *Nuclear Fusion* **55**

[31] Kishimoto H, Sakai N, Yamaji K, Horita T, Brito M E, Yokokawa H, Amezawa K and Uchitnoto Y 2008 Anomalous transport property at surface and interface of metal/rare earth doped ceria *Solid State Ionics* **179** 1343-6